

# You Only Train Once: A Unified Framework for Both Full-Reference and No-Reference Image Quality Assessment

Yi Ke Yun, *Student, IEEE* and Weisi Lin, *Fellow, IEEE*

**Abstract**—Although recent efforts in image quality assessment (IQA) have achieved promising performance, there still exists a considerable gap compared to the human visual system (HVS). One significant disparity lies in humans’ seamless transition between full reference (FR) and no reference (NR) tasks, whereas existing models are constrained to either FR or NR tasks. This disparity implies the necessity of designing two distinct systems, thereby greatly diminishing the model’s versatility. Therefore, our focus lies in unifying FR and NR IQA under a single framework. Specifically, we first employ an encoder to extract multi-level features from input images. Then a Hierarchical Attention (HA) module is proposed as a universal adapter for both FR and NR inputs to model the spatial distortion at each encoder stage. Furthermore, considering that different distortions contaminate encoder stages and damage image semantic meaning differently, a Semantic Distortion Aware (SDA) module is proposed to examine feature correlations between shallow and deep layers of the encoder. By adopting HA and SDA, the proposed network can effectively perform both FR and NR IQA. When our proposed model is independently trained on NR or FR IQA tasks, it outperforms existing models and achieves state-of-the-art performance. Moreover, when trained jointly on NR and FR IQA tasks, it further enhances the performance of NR IQA while achieving on-par performance in the state-of-the-art FR IQA. You only train once to perform both IQA tasks. Code will be released at: <https://github.com/BarCodeReader/YOTO>.

**Index Terms**—Full Reference IQA, No Reference IQA, Transformer, Unified Structure

## I. INTRODUCTION

The importance of accurately assessing image quality has become increasingly crucial in many fields [14], [38], [43], [71], [78]. Though the human vision system (HVS) is capable of identifying high-quality images effortlessly, it is labor-intensive, and in most cases infeasible, to assess image quality via human workers. Therefore, image quality assessment (IQA) aims to develop objective metrics that can predict image quality as perceived by humans [29].

Depending on the presence of high-quality reference images, IQA tasks can be grouped into two categories: No-Reference (NR) and Full-Reference (FR)<sup>1</sup>. Early studies apply hand-crafted metrics to perform the IQA. FR-IQA metrics like PSNR, SSIM [62], and NSER [73] assess image quality via signal fidelity and structural similarity between distorted and reference images. NR-IQA metrics such as DIIVINE [53] and BRISQUE [47] attempt to model natural scene statistics for quality measurement. These methods are well-defined

<sup>1</sup>In some papers IQA with partial reference, Reduced-Reference (RR), is introduced as the third category.

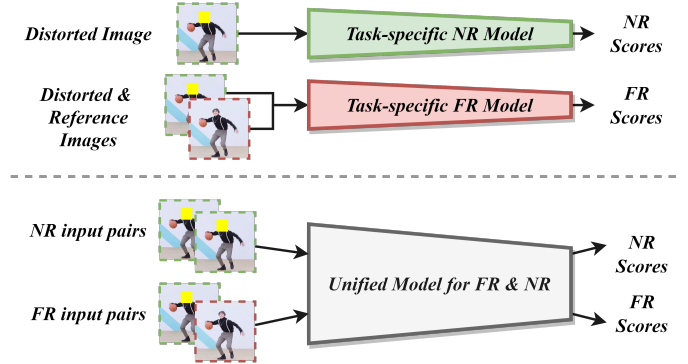


Fig. 1. Illustration of the main purpose for the proposed network (the lower part in the figure), where different image pairs can be fed into the network to yield FR/NR IQA scores using the same architecture. The traditional framework is given as the upper part of the figure for easy comparison. Our method offers great simplicity in both training and applications, minimizing performance inconsistencies on switching FR/NR tasks, and it achieves state-of-the-art performance on both FR and NR IQA benchmarks.

for specific distortions and are usually poorly generalized. Unlike other methods that compare distorted images with pristine images, BPRI [42] and BMPRI [44] aim to first obtain characteristics from the image that suffers the most distortion, namely pseudo-reference image (PRI), then estimate quality scores by the blockiness, sharpness, and noisiness between distorted images and PRIs.

In the deep learning era, the core idea for most FR-IQA methods is to estimate quality score by identifying low-quality regions through differencing the reference and distorted images or their extracted features [22], [52], [58]. For NR-IQA, common practices are adopting ranking [36], [48], [49], feature comparison [41], [63], generating pristine images using Generative Adversarial Networks (GAN) [5], [25], [33], [39], and applying Transformers or multi-scale CNNs for better spatial modeling of distortions [7], [14], [35], [57], [65], [67], [77]. The rationale behind these NR methods is to implicitly identify low-quality regions for IQA score estimation.

With or without the reference image, human beings can perform both FR and NR IQA effortlessly. This indicates that the FR and NR IQA share commonalities and there is a general model in our brains capable of performing both tasks. Recent research has found Saliency Map [3], [30], [54], [66] to be beneficial for both FR and NR IQA tasks. This serves as additional evidence demonstrating the commonalities between FR and NR IQA. Unfortunately, methods in the field are



Fig. 2. Illustration of how humans assess image quality when distortion is present: which one has the highest quality score? (a) a  $100 \times 100$  yellow block is presented in the background. (b) four blocks in both background and foreground (the basketball player). (c) a  $200 \times 200$  block in the background. (d) a  $100 \times 100$  block on the face. Quality score based on the amount of distortion: (b) < (a) and (c) < (a), while that based on the semantic impact to content (the player): (b) < (c) and thus (b) < (c) < (a). How about (d)? It has less amount of distortions than (b) and (c). However, it should have the lowest quality score because the most important message, the face, is damaged. Thus, aside from the amount, distortion is significant if it has critical damage to an image’s semantic meaning.

typically task-specific designed, as illustrated in Fig.1. They are indeed effective; however, once trained, they cannot be readily transferred to other IQA tasks (like from NR to FR or vice versa). Consequently, they lack a certain degree of generality and still exhibit a gap compared to humans, thus hindering our exploration of the underlying essence of IQA. A model capable of performing both IQA tasks can narrow this gap and thus it is meaningful and necessary. Besides, not only are human beings capable of perceiving the amount of distortion present in an image, but we are also adept at identifying the extent to which such distortion affects the semantic meaning, as illustrated in Fig.2. Though the field has recognized the significance of semantic information such as saliency, we lack an effective method for modeling the impact of distortion on semantic meaning.

To this end, we aim to narrow the gap between FR and NR IQA by developing a unified model and to improve existing IQA performance from the perspective of semantic modeling of distortion. Specifically, we first apply an encoder (ResNet50 [18] or Swin Transformer [37]) for feature extraction. Input images are encoded into multi-scale features. We then utilize the attention mechanism as the universal adaptor for FR and NR tasks. Depending on the input pairs, i.e.  $\{distorted\ img.,\ distorted\ img.\}$  or  $\{distorted\ img.,\ pristine\ img.\}$ , the attention block can dynamically switch between self-attention and cross-attention thus unifying FR and NR tasks. However, global attention is usually sparse due to the large spatial dimension of shallow features. To further model the spatial distortion, by applying a scale factor  $r$ , we partitioned the attention matrix into patches and computed the local attention. We stack several attention blocks together with different scale factors and name it the Hierarchical Attention (HA) module. To model the semantic impact caused by distortion, we developed a Semantic Distortion Aware (SDA) module. Distortions at one encoder stage, based on their types and strengths, might remain and affect the next few encoder stages differently. Though self-attention is effective in identifying spatially spread distortions, it has a weak representation of how distortions are correlated across all encoder stages. To this end, we propose to compute the cross-attention between features from different encoder stages. To ensure efficiency, the calculation is performed only between

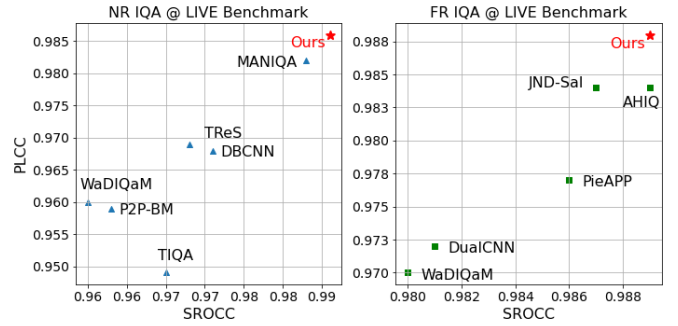


Fig. 3. Performance comparison against other FR and NR IQA models on LIVE [55] dataset. Our method achieves state-of-the-art performance on both FR and NR IQA benchmarks using the same network architecture.

high-level feature pixels and their associated low-level sub-regions (like a "cone"). Lastly, features from HA and SDA are concatenated and aggregated for quality score generation.

Extensive experiments on four FR-IQA benchmarks and seven NR-IQA benchmarks demonstrate the effectiveness of our proposed network. The proposed network outperforms other state-of-the-art methods on both FR and NR tasks using a unified architecture, as shown in Fig.3. To sum up, our contributions are threefold as follows:

- We propose a unified framework, YOTO, for both FR and NR IQA tasks and achieve state-of-the-art performance. The unified structure offers great simplicity and to our best knowledge, we are the first to aim to complete these two tasks using the same network architecture for IQA.
- We introduce the Hierarchical Attention (HA) module as the universal adaptor for both NR and FR inputs and for spatial distortion modeling. We further devise a Semantic Distortion Aware (SDA) module for semantic impact modeling.
- The unified network also enables joint training on both FR and NR IQA. **You only train once**, and the obtained model can achieve on-par performance on the FR task and better performance on the NR task trained separately.

## II. RELATED WORK

**FR-IQA** Since reference images are given alongside distorted images, the core idea is to estimate the quality scores based on the differences. The most straightforward way is to calculate the Mean-squared Error (MSE) between distorted images and reference images. However, MSE cannot effectively reflect visual quality perceived by humans [13] and various image quality metrics have been developed striving for better alignment with HVS [34]. With the emergence of deep learning, DeepQA [22] applies CNN on distorted images and their corresponding difference maps to estimate quality scores. Similarly, DualCNN [58] and PieAPP [52] perform IQA based on the feature differences between pristine images and distorted images. These methods focus on modeling spatial differences but ignore the semantic impacts caused by distortion. To mitigate this issue, saliency was introduced to reflect visually important regions [1], [21], [54], [75]. However, saliency is simply served as an attention map and usually

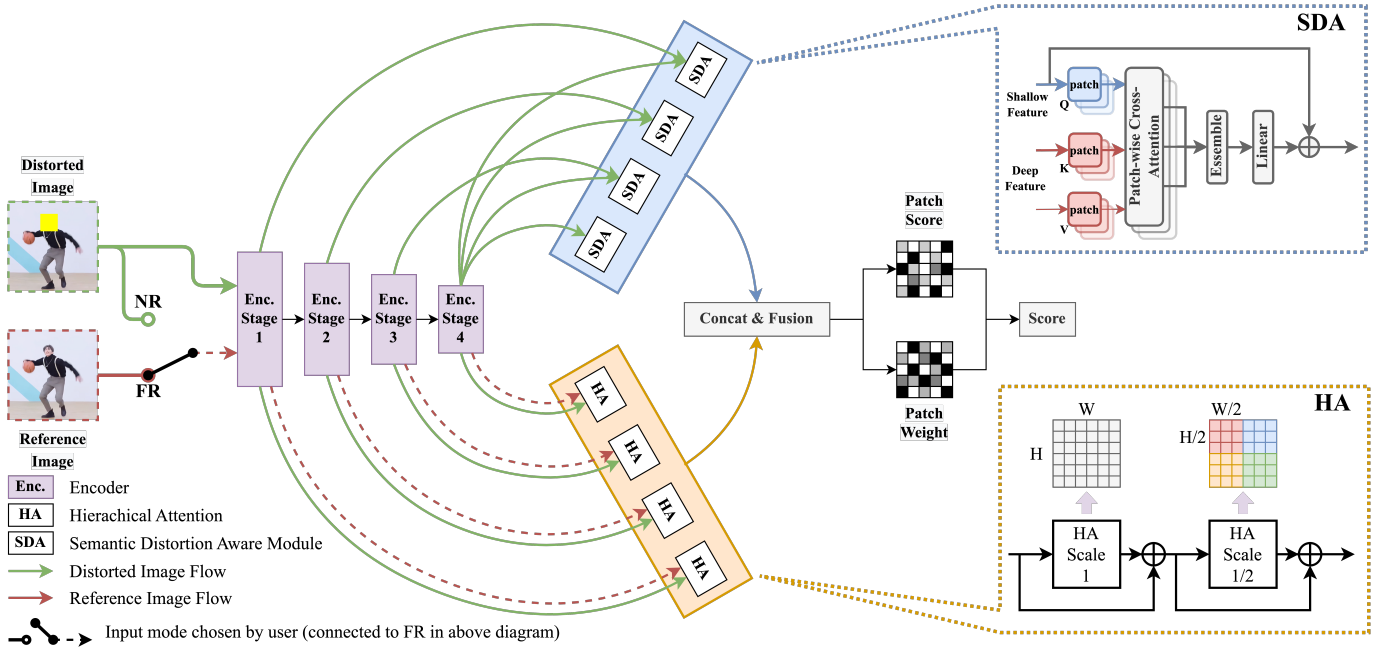


Fig. 4. Network architecture of the proposed YOTO. Input types can be chosen by the user depending on the presence of reference images for the network to perform FR or NR IQA tasks (i.e. the dotted red arrow will become green if the user chooses to perform NR IQA). The network receives a pair of images in the form of  $[distorted, distorted]$  or  $[distorted, reference]$  for NR and FR IQA respectively. ResNet50 or Swin Transformer is adopted as the encoder backbone (purple). A Hierarchical Attention (HA) module with global and regional attention is developed to highlight potential distortion-contaminated areas in encoder features. If only distorted images are provided, self-attention is applied in the HA module. If reference images are given, the HA module will compute the cross-attention between distorted and reference features. To model the semantic impact caused by distortion, a Semantic Distortion Aware (SDA) module is designed and densely applied to explore the similarity between shallow and deep features using only distorted image features. The obtained features from HA and SDA are concatenated and fused for IQA score estimation via a commonly applied patch-wise attention. Best viewed in color.

requires an extra saliency network for saliency generation. Thus better modeling of semantic impact caused by distortion still awaits more investigation.

**NR-IQA** One of the ideas for NR IQA is to generate the reference image using GAN-based methods [33], [39] to transform NR into FR tasks. However, the performance of this approach is greatly bottlenecked by the GAN itself. Without explicitly generating reference images, similar to FR IQA, saliency [66] is usually considered as auxiliary information for better quality score estimation. Alternatively, ranking [36], [60] is commonly applied to implicitly learn the distortion level in images using Siamese networks. Besides, Vision Transformers [8], [14], [60], [67], [70] are adopted to capture better spatial relationships aiming to identify hidden distortion patterns. Although the aforementioned methods share great similarities with FR IQA, most networks are typically designed only for NR tasks. An ideal model should be able to perform both FR and NR IQA tasks, just like human beings. To our best knowledge, the only method [3] reporting performances on both NR and FR benchmarks still requires modifications of its network architecture, and its performance is inferior to the latest single-task models. Hence, the exploration of a unified model is non-trivial, as it can narrow the gap between current models and human capabilities, while also inspiring and facilitating a better exploration of underlying principles between FR and NR IQA.

**Cross-attention** Cross-attention was originally introduced in Natural Language Processing (NLP) to translate a source

language to another (eg., English to French) [59]. Due to its ability to examine correlations between different modalities, it has been widely adopted in various NLP and computer vision applications, such as text and image matching [28], [64]. It is also widely applied in Transformers for multi-scale image feature correlation modeling [6], [31]. For IQA tasks, various self-attention-related models have been proposed thanks to the long-range dependency modeling capability of transformers [8], [26], [60], [67]. The self-attention is applied at each encoder stage and the resulting weighted features are effective in identifying distortion in spatial dimensions. However, part of the distortion at one encoder stage might remain and continue to affect the next few encoder stages. This part of features should gain higher attention consistently as they have greater impacts on the semantics of the image. Thus solely applying self-attention for each encoder stage cannot effectively reflect the semantic impact caused by distortion. Cross-attention, on the other side, is not well investigated yet and seems a promising solution for semantic impact modeling. Since different types of distortion will contaminate encoder layers differently, we can apply cross-attention to calculate correlations between shallow features and deep features to estimate the strength of distortion affecting the semantic meaning of an image.

### III. PROPOSED METHOD

#### A. Overall Architecture

The overall architecture is shown in Fig.4. We adopt ResNet [18] or Swin Transformer [37] as our encoder backbone for image feature encoding. The encoder is shared if reference images are present. Channel-wise attention is applied to encoder features. After that, a Hierarchical Attention (HA) module is developed to be an adaptor for NR and FR inputs and to identify potentially damaged regions in encoder features. The self-attention employed in the HA module will become cross-attention if pristine image features are present. Therefore the network is capable of receiving both FR and NR inputs. Furthermore, a Semantic Distortion Aware (SDA) module is proposed to estimate the semantic impact caused by distortion presented in the image. Finally, an aggregation block with patch-wise attention is devised for quality scores.

#### B. Hierarchical Attention (HA)

In order to simultaneously address FR and NR IQA tasks, a network requires an adaptive input processing module. The module should be capable of dynamically adjusting the calculation based on the presence or absence of reference images. In this regard, the attention mechanism from the original Transformer [59] is considered as a potential solution. When only distorted images are available, self-attention can be utilized to enable the network to identify the possible locations of distortion and adjust the weight of features accordingly. On the other hand, if pristine images are provided in addition to distorted images, cross-attention can be employed to achieve the same objective without increasing computational complexity. Denote the distorted features and reference features as subscripts  $dis$  and  $ref$ , the attention devised can be described as:

$$Attention = \begin{cases} Softmax(\frac{Q_{dis}K_{dis}^T}{\sqrt{d_{head}}})V_{dis}, & \text{if NR.} \\ Softmax(\frac{Q_{ref}K_{dis}^T}{\sqrt{d_{head}}})V_{dis}, & \text{if FR.} \end{cases} \quad (1)$$

where  $Q, K, V$  are embeddings calculated by different MLP layers.

However, the network has no idea which and when the pristine image is present in the input pairs. To this end, we introduce a segmentation embedding layer  $embd(\cdot)$  indicating the input information of FR and NR IQA, as shown in Fig.5. After embedding, with the developed HA, the network can now perform both NR and FR tasks automatically based on different input image pairs:

$$score = \begin{cases} \mathcal{F}(embd(\mathbf{0}) + x_{dis}, embd(\mathbf{0}) + x_{dis}), & \text{if NR.} \\ \mathcal{F}(embd(\mathbf{0}) + x_{dis}, embd(\mathbf{1}) + x_{ref}), & \text{if FR.} \end{cases} \quad (2)$$

where  $x_{dis}$  and  $x_{ref}$  denotes distorted and reference images,  $\mathcal{F}$  stands for the network and  $\{\mathbf{0}, \mathbf{1}\}$  are embedding vectors.

The adoption of attention resolves the issue of different inputs for FR and NR IQA. When computing attention on the encoder features, the attention matrix formed by patch embeddings can become quite large due to the typically large spatial dimension of shallow features. For example, a  $512 \times 512$

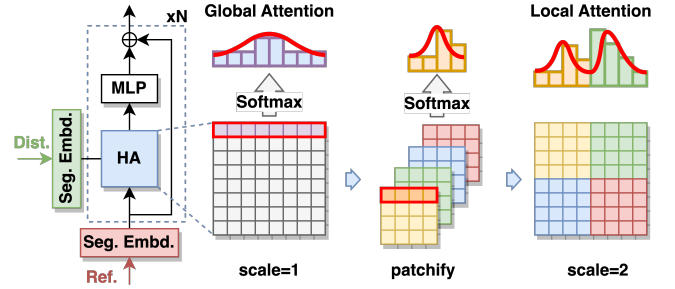


Fig. 5. The developed Hierarchical Attention (HA) module that bridges FR and NR tasks together. Segmentation embeddings were added to input features as an indicator of NR and FR tasks. Depending on FR or NR tasks, the input pair shown above could be  $\{distortion, reference\}$  or  $\{distortion, distortion\}$  respectively. Besides, on top of global attention, we partitioned the attention matrix into patches to incorporate local attention as well. In practice, the HA module will stack multiple attention layers with different scale factors to fully exploit global and local attention.

single-channel image split into non-overlapping patches of  $16 \times 16$  will give a sequence of  $32 \times 32 = 1024$  in length and result in an attention matrix of  $1024 \times 1024$ . As a result, after applying softmax to each row, the attention scores between patches might be very similar, leading to an indistinct weighting effect on the features. NLP and ViT models commonly resolve this problem by stacking multiple attention layers. However, this approach may not be efficient in terms of computation cost and convergence speed. To this end, we partition the feature maps into blocks and compute attention for each block separately, and then concatenate the resulting attention matrices into a large matrix. **Please note our approach has a distinct difference from Multi-head Self-attention (MSA) [59] as we split features from shape  $[Batch, Length, Channels]$  to  $[Batch, scale^2, Length/scale^2, Channels]$  while in MSA the channel dimension is split.** As we can choose different scale factors to divide the original matrix into various sizes of blocks, we name the designed module Hierarchical Attention (HA). With this approach, both global and local attention are exploited. Mathematically, given an input sequence  $x \in R^{B \times HW \times C}$ , a scale factor  $r$  will split the attention matrix  $M \in R^{B \times HW \times HW}$  into  $r^2$  blocks  $M_{ij}$  where  $i, j \in [0, r)$ . Defining the operation  $P_{i,j=0}^{r-1} M_{ij}$  to paste the attention matrix  $M_{ij}$  back to the original matrix  $M$  following its coordinate  $[i, j]$ , a single layer of HA can be calculated as:

$$Q_{r,ij}, K_{r,ij} \in R^{B \times (r)^2 \times HW / (r)^2 \times C} \quad (3)$$

$$M_{ij} = Softmax(\frac{Q_{r,ij}K_{r,ij}^T}{\sqrt{d_{head}}}) \quad (4)$$

$$M = P_{i,j=0}^{r-1} M_{ij} \quad (5)$$

$$HA(x_t, r) = x_t + MLP(MV), \quad V \in R^{B \times HW \times C} \quad (6)$$

The HA module can be described recursively:

$$HA(x_{t+1}, r) = HA(HA(x_t, r), r), \quad t = 0, 1, \dots \quad (7)$$

The overall design of the HA module is illustrated in Fig.5 where we stack multiple HA layers with different scale factors and apply residual connections. The effectiveness of the HA module will be discussed more in ablations.



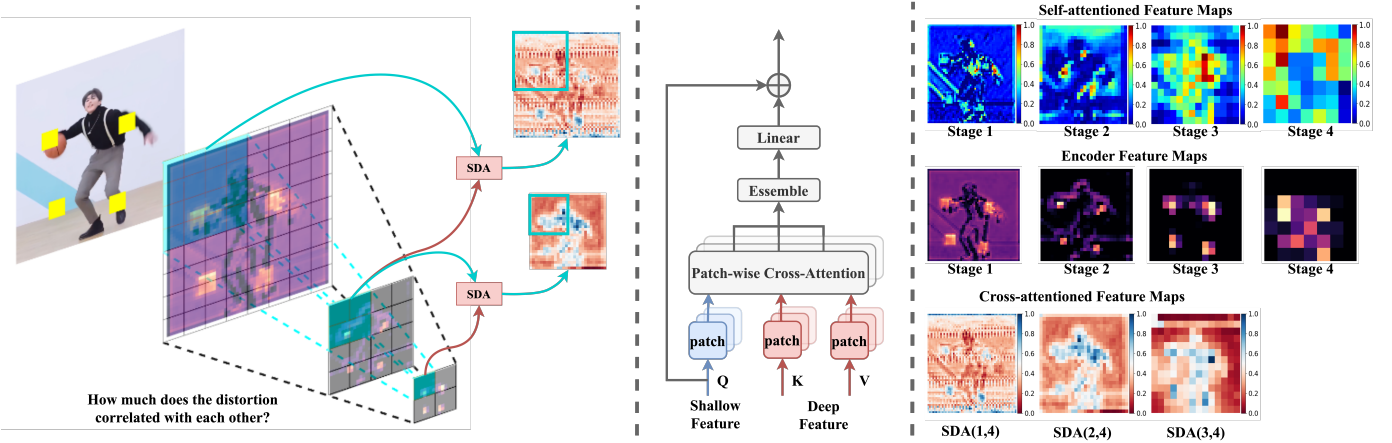


Fig. 6. Illustration of SDA (left and middle) and comparison against self-attention (right). Feature pyramid is firstly split into  $n \times n$  cones. The SDA is then densely applied on encoder stages to explore the correlation between shallow and deep features so that we can estimate the semantic impact caused by distortion. SDA(1,4) denotes the weighted feature map obtained by computing cross-attention between stages 1 and 4. As illustrated on the right side, the cross-attention feature maps (last row) can reflect how distortions in shallow stages are related to the deep features, further indicating the impact the distortion caused. Self-attention features (first row), on the other side, indicate the important region in space but are inconsistent across different encoder stages and thus have a weak representation of semantic impact.

### C. Semantic Distortion Aware (SDA) Module

The HA module provides effective attention allowing the model to focus on certain regions of the image. However, as mentioned in the previous sections, relying solely on the amount of distortion in the image may not adequately reflect image quality as we ignored the impact distortion applied on deeper encoder layers. Thus, we need to assess the damage to the semantic information caused by distortion for better evaluation. Considering that the encoder itself is a natural feature extractor or feature summarizer, i.e., the details and textures in the image are gradually filtered out during the encoding process, leaving behind high-level semantic information such as location. Based on this characteristic, we propose to evaluate the amount of semantic impact caused by different types of distortion by examining their residual effects in each encoder layer. Different from common approaches [14], [56], [76] where features are aggregated or scores are averaged, we aim to estimate the semantic damage caused by the distortions from the perspective of feature consistency. The distortion that affects the next few stages of the encoder should receive more attention. For instance, we believe the impact of salt-and-pepper distortion and block occlusion will reach different layers when they pass through the encoder. Salt-and-pepper distortion is likely to be filtered out effectively in the first few layers of the encoder, while block occlusion may penetrate till the last layer of the encoder, affecting the semantics of the entire image.

We propose using cross-attention between different encoder layers to capture the impact of distortion on semantic meaning. By comparing the feature similarities between shallow and deep layers, we estimate the distortion residues in different layers and evaluate image quality. Therefore, we design the Semantic Distortion Aware (SDA) module, as shown in Fig.6. It is a cross-attention module in a top-down manner and is densely applied between different encoder features. At first glance, the proposed SDA might look superficially simple. **In**

**fact, instead of blindly applying the cross-attention, we partition the feature pyramid into a "cone" and trace a local patch from shallow to deep features to estimate the semantic correlations.** This design prevents meaningless interactions between a local distortion and its high-level neighbor regions during cross-attention. It bridges low-level and high-level features, focusing on how local distortions within low-level features affect high-level semantics. Meanwhile, it is more computationally efficient ( $1/n^2$  if has  $n \times n$  cones) compared with full-scale attention. The SDA module uses shallow features as queries  $Q_s$  and deep features as keys  $K_d$  and values  $V_d$  to calculate the weighted map of shallow-layer features, reflecting which region on the image has a direct correlation and persistent effect on its deep semantic meanings. Given shallow and deep features  $x_s, x_d$  with batch  $B$ , channel  $C$  and spatial dimension  $m \times m$  and  $n \times n$ , then we have:

$$x_s \in R^{B \times (m \times m) \times C}, \quad x_d \in R^{B \times (n \times n) \times C}, \quad m > n$$

$$Attention(Q_s, K_d, V_d) = Softmax\left(\frac{Q_s K_d^T}{\sqrt{d_{head}}}\right) V_d \quad (8)$$

$$SDA(x_d, x_s) = x_s + MLP(Attention(Q_s, K_d, V_d))$$

For each encoder stage 1–4, we apply HA to obtain features  $H_1, H_2, H_3$ , and  $H_4$  accordingly. Similarly, we densely apply SDA between encoder stage  $i$  and its shallower stages  $j$  ( $j < i$ ) to obtain correlation features,  $C_{i,j}$ . This will yield in  $C_{4,3}, C_{4,2}, \dots, C_{2,1}$  in total six feature groups. The obtained features from the same encoder stage  $i$  are averaged and concatenated along the channel dimension followed by a commonly applied patch-wise attention block [3], [26], [67] to predict quality scores, as shown in Fig.4.

### D. Training Schemes

Due to the proposed model architecture's ability to dynamically transform computation methods by accepting FR and NR IQA inputs, we have explored the possibility of conducting

joint training for FR and NR alongside traditional task-specific training. FR and NR inputs are provided to the model with a probability of 50% in a format of  $\{distortion, reference\}$  or  $\{distortion, distortion\}$ . **We found that, compared to separate training, joint training not only achieves similar performance in FR but also significantly enhances NR performance.** Further details will be presented in the experiments and ablation analyses.

## IV. EXPERIMENTS

### A. Datasets and Metrics

We evaluate our algorithm on conventional seven NR benchmark datasets and four FR benchmark datasets. In addition, we also report the results on the PIPAL [15] dataset consisting of GAN-generated images. For NR benchmarks, four synthetic distorted datasets, TID2013 [51], LIVE [55], CSIQ [27], and Kadid10k [32] are adopted. These synthetic distorted datasets are also employed for FR evaluations. Besides, we use three authentic datasets, namely LIVE Challenge [12], KonIQ10k [19], and LIVEFB [68], to further test our model’s performance on NR tasks.

**TID2013:** TID2013 dataset contains 3000 distorted images derived from 25 pristine images with 24 different distortion types at 5 degradation levels. Mean Opinion Scores are ranging from 0 to 9.

**LIVE:** Live degrades 29 pristine images by adding additive white Gaussian noise, blurring Gaussian, compressing JPEG, compressing JPEG2000, and fast fading, resulting in 770 distorted images in total.

**CSIQ:** The dataset contains 886 distorted images originating from 30 pristine images. The CSIQ database includes six types of distortions, each with four or five levels of distortion respectively.

**Kadid10K:** This dataset contains 10,125 images that have been degraded based on 81 pristine images. Five levels of distortion are applied to each pristine image.

**KONIQ-10K:** The KONIQ-10K dataset consists of 10,073 images covering a wide variety of images from various domains, including nature, people, animals, and objects. Each image in KONIQ-10K is rated on a scale from 1 to 10.

**LIVE-Challenge:** The LIVE-Challenge dataset consists of 1,160 distorted images. The distortions include compression artifacts, noise, blurring, and other types of impairments.

**LIVE-FB:** The LIVE-FB dataset is the largest in-the-wild NR-IQA dataset by far and it contains around 40 thousand distorted images and 1.2 million image patches labeled by crowd-sourcing.

**PIPAL:** The PIPAL dataset introduces GAN-generated images as a new distortion type. Unlike conventional distortion types, the outputs from GAN-based models follow the natural image distribution quite well but with the wrong details. The PIPAL dataset consists of 250 pristine images with 40 distortion types and in total over 1 million labelings.

For metrics, we adopt Pearson’s Linear Correlation Coefficient (PLCC) and Spearman’s Rank Order Correlation Coef-

ficient (SROCC) as our evaluation metrics. PLCC is defined as:

$$PLCC = \frac{\sum_{i=1}^n (x_i - \bar{x})(y_i - \bar{y})}{\sqrt{\sum_{i=1}^n (x_i - \bar{x})^2 (y_i - \bar{y})^2}} \quad (9)$$

where  $x_i, y_i$  indicate the predicted and the ground truth scores, and their mean values are denoted as  $\bar{x}, \bar{y}$  respectively. Meanwhile, SROCC is defined as:

$$SROCC = \rho = 1 - \frac{6 \sum d_i^2}{n(n^2 - 1)} \quad (10)$$

where  $n$  is the total number of samples, and  $d_i$  is the rank difference of the  $i^{th}$  test image between ground-truth and predictions.

### B. Implementation Details

For the PIPAL dataset, we follow their official split and training protocols mentioned in the paper. For the other datasets mentioned in Sec.IV-A, we randomly sample 80% of the data as the training dataset and the rest as the testing dataset. We choose ResNet50 and Swin Transformer as our encoder backbone to compare with other CNN and transformer models respectively. During training, images are augmented by random cropping with a size of  $224 \times 224$  and random horizontal flipping by 50% chance. The learning rate is set to  $1e^{-4}$  using the CosineAnnealing scheduler with  $Tmax$  and  $eta\_min$  set to 50 and 0, respectively. We use a batch size of 8 and Adam optimizer [24] with default parameters. The network is trained using L2 loss for 100 epochs. During testing, each image is randomly cropped into  $224 \times 224$  for 20 times, and their averaged prediction scores are calculated. We train the network 5 times using different seeds and report the mean value. *Code will be released upon acceptance.*

### C. Comparisons with the State-of-the-art

**Single Task Training** We compare our proposed YOTO against 13 NR IQA algorithms in the field, namely DIVINE [53], BRISQUE [47], ILNIQE [72], BIECON [23], MEON [40], WaDIQaM [4], DBCNN [74], MetaIQA [76], P2P-BM [69], HyperIQA [56], TReS [14], TIQA [70], and MANIQA [67]. ResNet50 and Swin Transformer are used as our backbones respectively in order to compare the performance of other ResNet50-based and Transformer-based models. As listed in Tab.I, our proposed network outperforms other algorithms on both ResNet-base and Transformer-based architectures.

Besides, we compare YOTO against 6 FR IQA methods, which are DOG [50], DeepQA [22], DualCNN [58], WaDIQaM [3], PieAPP [52], and AHIQ [26]. As shown in Tab.II, our proposed method performs in line with the current state-of-the-art model AHIQ, which indicates the effectiveness of our proposed unified architecture on IQA tasks. Moreover, predicted quality scores shown in Tab.IV further indicate our proposed YOTO performing well on both FR and NR tasks. The predicted IQA scores can correctly align with the MOS ranking based on HVS.

In addition to the above FR and NR benchmarks, we also trained YOTO on the PIPAL dataset. As shown in Tab.III,

TABLE I

QUANTITATIVE COMPARISON BETWEEN OUR PROPOSED NR-IQA NETWORK AND OTHER STATE-OF-THE-ART NR-IQA METHODS. POSTFIX **-R** AND **-S** STANDS FOR MODEL TRAINED ON NR TASK ONLY WITH RESNET50 AND SWIN-TINY TRANSFORMER ENCODER BACKBONE, RESPECTIVELY. MODEL END WITH † IS JOINTLY TRAINED UNDER FR & NR TASKS. OUR JOINTLY TRAINED MODEL ACHIEVES BETTER PERFORMANCE ON NR TASKS.

Methods	LIVE		CSIQ		TID2013		KADID10K		LIVE-C		KonIQ10K		LIVEFB	
	PLCC	SROCC	PLCC	SROCC	PLCC	SROCC	PLCC	SROCC	PLCC	SROCC	PLCC	SROCC	PLCC	SROCC
DIIVINE	0.908	0.892	0.776	0.804	0.567	0.643	0.435	0.413	0.591	0.588	0.558	0.546	0.187	0.092
BRISQUE	0.944	0.929	0.748	0.812	0.571	0.626	0.567	0.528	0.629	0.629	0.685	0.681	0.341	0.303
ILNIQE	0.906	0.902	0.865	0.822	0.648	0.521	0.558	0.528	0.508	0.508	0.537	0.523	0.332	0.294
BIECON	0.961	0.958	0.823	0.815	0.762	0.717	0.648	0.623	0.613	0.613	0.654	0.651	0.428	0.407
MEON	0.955	0.951	0.864	0.852	0.824	0.808	0.691	0.604	0.710	0.697	0.628	0.611	0.394	0.365
WaDIQaM	0.955	0.960	0.844	0.852	0.855	0.835	0.752	0.739	0.671	0.682	0.807	0.804	0.467	0.455
DBCNN	0.971	0.968	0.959	0.946	0.865	0.816	0.856	0.851	0.869	<b>0.869</b>	0.884	0.875	0.551	0.545
MetaIQA	0.959	0.960	0.908	0.899	0.868	0.856	0.775	0.762	0.802	0.835	0.856	0.887	0.507	0.540
P2P-BM	0.958	0.959	0.902	0.899	0.856	0.862	0.849	0.840	0.842	0.844	0.885	0.872	0.598	0.526
HyperIQA	0.966	0.962	0.942	0.923	0.858	0.840	0.845	0.852	0.882	0.859	0.917	0.906	0.602	0.544
TReS	0.968	0.969	0.942	0.922	0.883	0.863	0.858	0.859	0.877	0.846	<b>0.928</b>	0.915	0.625	0.554
<b>Ours-R</b>	<b>0.976</b>	<b>0.974</b>	<b>0.962</b>	<b>0.952</b>	<b>0.908</b>	<b>0.902</b>	<b>0.884</b>	<b>0.885</b>	<b>0.892</b>	0.841	0.925	<b>0.917</b>	<b>0.637</b>	<b>0.563</b>
<b>Transformer-based</b>														
TIQA	0.965	0.949	0.838	0.825	0.858	0.846	0.855	0.850	0.861	0.845	0.903	0.892	0.581	0.541
MANIQA	0.983	0.982	0.968	0.961	0.943	0.937	0.939	0.939	-	-	-	-	-	-
<b>Ours-S</b>	<b>0.986</b>	<b>0.986</b>	<b>0.970</b>	<b>0.964</b>	<b>0.956</b>	<b>0.953</b>	<b>0.942</b>	<b>0.941</b>	<b>0.903</b>	<b>0.869</b>	<b>0.938</b>	<b>0.926</b>	<b>0.652</b>	<b>0.570</b>
<b>Ours-S†</b>	<b>0.987</b>	<b>0.987</b>	<b>0.977</b>	<b>0.976</b>	<b>0.958</b>	<b>0.956</b>	<b>0.945</b>	<b>0.944</b>	-	-	-	-	-	-

our proposed model with a Swin-Tiny backbone achieved on-par performance against the state-of-the-art MANIQA and AHIQ. Better scores were obtained when switching to a more powerful backbone, i.e. Swin-Small. Complexity-wise, the proposed YOTO has fewer parameters and MACs compared with the other state-of-the-art models, indicating the efficiency of our proposed method.

**Joint Training** We additionally present the metrics attained through joint training of the model on both NR and FR datasets. Results are shown in red in Tab.I and Tab.II. **Our model achieves commensurate performance with the FR task trained alone, while exhibiting a notable advancement over the NR task trained alone.** This observation underscores a shared characteristic between FR and NR tasks, suggesting that our proposed unified framework adeptly captures relevant hidden patterns during the joint training, thereby further boosting the performance of NR task.

## V. ABLATION STUDIES

**Effectiveness of the Proposed Modules** We reconfigured our network by switching on/off HA and SDA respectively and trained the network under TID2013 and CSIQ for both FR and NR IQA tasks. Evaluation results are listed in Tab.V. Compared with HA, the SDA module is more effective on IQA tasks. This is probably due to its effectiveness in modeling semantic damage across different stages, further indicating semantic damage is an important factor of IQA. When equipped with both models, the network yields the best performance. More detailed illustrations of feature maps from HA and SDA will be discussed in *Sec. Visualization of HA and SDA Module of ablation studies.*

**Effectiveness of Hierarchical Attention** In order to compare the effectiveness of the HA module, we fixed the scale

TABLE II

QUANTITATIVE COMPARISON BETWEEN YOTO AND OTHER FR METHODS IN THE FIELD. \* STANDS FOR TRANSFORMER-BASED METHODS. MODEL END WITH † IS JOINTLY TRAINED UNDER FR & NR TASKS WHILE MODEL END WITH \* IS TRAIN ON FR TASK ONLY. OUR JOINTLY TRAINED MODEL ACHIEVED ON-PAR PERFORMANCE OF FR IQA.

Methods	LIVE		CSIQ		TID2013		KADID10K	
	PLCC	SROCC	PLCC	SROCC	PLCC	SROCC	PLCC	SROCC
DOG	0.966	0.963	0.943	0.954	0.934	0.926	-	-
DeepQA	0.982	0.981	0.965	0.961	0.947	0.939	0.891	0.897
DualCNN	-	-	-	-	0.924	0.926	0.949	0.941
WaDIQaM	0.980	0.970	-	-	0.946	0.940	0.889	0.896
PieAPP	0.986	0.977	0.975	0.973	0.946	0.945	-	-
AHIQ*	<b>0.989</b>	0.984	0.978	0.975	<b>0.968</b>	0.962	-	-
<b>Ours*</b>	<b>0.989</b>	<b>0.988</b>	<b>0.979</b>	<b>0.979</b>	0.965	<b>0.963</b>	<b>0.950</b>	<b>0.943</b>
<b>Ours†</b>	<b>0.988</b>	<b>0.988</b>	<b>0.978</b>	<b>0.977</b>	<b>0.964</b>	<b>0.963</b>	<b>0.950</b>	<b>0.944</b>

TABLE III

QUANTITATIVE COMPARISON BETWEEN YOTO AND SOTA NETWORKS ON THE PIPAL TEST DATASET, WITH FLOPS AND PARAMETERS INDICATED. THE SUFFIX -T AND -S REPRESENTS SWIN TINY AND SMALL BACKBONES. OUR YOTO ACHIEVED GREAT PERFORMANCE WITH MUCH FEWER PARAMETERS AND MACS, INDICATING THE EFFECTIVENESS OF THE PROPOSED ARCHITECTURE.












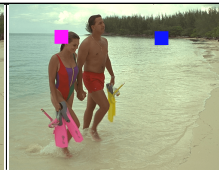
Methods	Params. (M)	MAC (G)	PIPAL (NR)		PIPAL (FR)	
			PLCC	SROCC	PLCC	SROCC
MANIQA	127.73	108.62	0.667	0.702	-	-
AHIQ	132.62	168.98	-	-	0.823	0.813
Ours-T	76.64	80.56	0.662	0.696	0.818	0.807
Ours-S	<b>105.36</b>	<b>98.62</b>	<b>0.669</b>	<b>0.703</b>	<b>0.826</b>	<b>0.815</b>

factor  $r$  to 1 and stacked the attention layer 2,4, and 6 times. Experiment results are listed in Tab.VI. In comparison to 6



TABLE IV

QUALITY SCORE COMPARISON FOR YOTO IN FR AND NR MODE AGAINST OTHER STATE-OF-THE-ART MODELS AHIQ (FR) AND MANIQA (NR). IMAGES ARE CHOSEN FROM THE TID2013 TEST SET WITH BLOCK OCCLUSION DISTORTION TYPE. FROM LEFT TO RIGHT: THE PRISTINE IMAGE AND 5 DISTORTED IMAGES WITH DESCENDING DISTORTION LEVELS. DIFFERENT COLOR CODES ARE APPLIED FOR BETTER VISUALIZATION OF THE 1ST, 2ND, 3RD, 4TH, AND 5TH RANKING OF PREDICTION SCORES.

					
Reference Image	Distortion 1	Distortion 2	Distortion 3	Distortion 4	Distortion 5
MOS (normed)	0.3959 (5th)	0.4181 (4th)	0.4382 (3rd)	0.4742 (2nd)	0.5566 (1st)
YOTO (FR)	0.4890 (5th)	0.4912 (4th)	0.4939 (3rd)	0.5031 (2nd)	0.5771 (1st)
YOTO (NR)	0.4823 (5th)	0.4937 (4th)	0.5000 (3rd)	0.5308 (2nd)	0.5636 (1st)
AHIQ (FR)	0.4901 (5th)	0.4945 (4th)	0.5104 (3rd)	0.5713 (1st)	0.5628 (2nd)
MANIQA (NR)	0.5112 (4th)	0.4996 (5th)	0.5644 (2nd)	0.5364 (3rd)	0.5709 (1st)
					
Reference Image	Distortion 1	Distortion 2	Distortion 3	Distortion 4	Distortion 5
MOS (normed)	0.4400 (5th)	0.4435 (4th)	0.4574 (3rd)	0.4948 (2nd)	0.5379 (1st)
YOTO (FR)	0.4242 (5th)	0.4930 (4th)	0.5056 (3rd)	0.5280 (2nd)	0.6165 (1st)
YOTO (NR)	0.4111 (5th)	0.4532 (4th)	0.4757 (3rd)	0.5616 (2nd)	0.6124 (1st)
AHIQ (FR)	0.4694 (5th)	0.5102 (3rd)	0.4811 (4th)	0.5709 (1st)	0.5598 (2nd)
MANIQA (NR)	0.4776 (4th)	0.4380 (5th)	0.5083 (3rd)	0.5702 (1st)	0.5349 (2nd)

layers of plain attention, two layers of HA with scale factors 1 and 2 produce competitive results. The HA module is efficient in computation and effective in performance. Besides, as the scale factor increases, the improvement of HA becomes marginal. This is probably because a large scale factor  $r$  will generate small attention blocks, which result in similar scores in each block and thus hinder the performance.

**Visualization of HA and SDA Module** We investigate the effectiveness of our proposed HA and SDA module by visualizing encoder features and the attention matrix learned. ResNet50 version of YOTO is used, as shown in Fig.7 and Fig.8. We choose two typical distortion patterns in this analysis, specifically, Block Occlusion Distortion and Sparse Sampling. Feature maps are sampled at the same channel position of each encoder layer for both reference images and distorted images. Visualizations reflect the fact that mild distortion will be filtered out by the shallow encoder layers while severe distortion will persist and ultimately affect the deepest layer of features. The proposed HA and SDA modules can effectively reflect the amount of spatial distortion and the correlation between shallow and deep features, which can help the network estimate quality scores.

**Cross-dataset Evaluation** Following prior research [26], [67], we also perform cross-dataset evaluation by training our model on KADID-10K and LIVE and testing on CSIQ and TID2013 respectively for both FR and NR tasks. As shown in Tab.VIII, our proposed network achieves acceptable generalization ability on both FR and NR tasks.

**Mix-dataset Joint Training** A more comprehensive eval-

uation is conducted by jointly training our model on different FR and NR datasets. We combined one authentic NR dataset and two synthetic FR datasets to train our model and evaluate it under NR IQA. The network will receive FR image pairs (*distorted, reference*) or NR image pairs (*distorted, distorted*) depending on the sampling. For NR models like MANIQA and TReS, only NR image pairs are loaded. The train/test split ratio is 0.8 for each dataset and we train the network for 200 epochs with a learning rate of  $1e^{-4}$ . The experiment results shown in Tab.VII demonstrate that our model is still able to achieve fairly good performance and outperform other single-task models with **up to 10% performance increment** using this joint training strategy with a mixed dataset.

## VI. DISCUSSION

**Necessity of a Unified Model** Human perception of image quality relies significantly on the interaction of various modalities of information, such as visual, textual, and auditory cues. Recent research endeavors have begun integrating additional modalities, such as audio [45], [46], into this domain. Hence, in the long term, IQA models are envisioned to integrate diverse modalities within a unified architecture. Our work represents an initial step in this direction by unifying NR and FR IQA. This integration not only reduces the current disparities between FR and NR IQA models but also lays the groundwork for a scalable backbone for future multimodal endeavors.



TABLE V  
ABLATION STUDY ON THE EFFECTIVENESS OF HA AND SDA MODULE ON FR AND NR TASKS.

Configuration			TID2013 (NR)		CSIQ(NR)		TID2013 (FR)		CSIQ(FR)	
HA	SDA (no cone)	SDA (cone)	PLCC	SRCC	PLCC	SRCC	PLCC	SRCC	PLCC	SRCC
✓			0.946	0.943	0.961	0.952	0.953	0.949	0.966	0.968
	✓		0.944	0.944	0.960	0.950	0.950	0.948	0.964	0.965
		✓	0.949	0.947	0.966	0.958	0.958	0.955	0.971	0.972
✓		✓	<b>0.956</b>	<b>0.953</b>	<b>0.970</b>	<b>0.964</b>	<b>0.965</b>	<b>0.963</b>	<b>0.979</b>	<b>0.979</b>

TABLE VI  
EFFECTIVENESS OF THE HA MODULE. LEFT HALF: BY FIXING THE SCALE FACTOR  $r = 1$ , HA BECOMES PLAIN ATTENTION. MULTIPLE HA LAYERS ARE STACKED AND THEIR RESULTS ARE REPORTED. RIGHT HALF: HA MODULE WITH DIFFERENT SCALE FACTOR SETTINGS. AS SHOWN BELOW, HA(1,2) PERFORMS BETTER THAN 6 LAYERS OF PLAIN ATTENTION.

HA(r=1)	TID2013		CSIQ		HA(r)	TID2013		CSIQ	
No. Layers	PLCC	SROCC	PLCC	SROCC		PLCC	SROCC	PLCC	SROCC
2	0.948	0.941	0.953	0.948	HA(1,2)	0.956	0.953	0.970	0.964
4	0.951	0.946	0.958	0.951	HA(1,2,4)	0.953	0.948	0.962	0.955
6	0.953	0.949	0.966	0.975	HA(1,2,4,8)	0.950	0.946	0.957	0.949

TABLE VII  
MIX-DATASET EVALUATION. THE MODEL WAS TRAINED ON THE MIXED TRAINING DATASET OF {LIVE, CSIQ, KONIQ-10K} AND {TID2013, KADID-10K, LIVE-C}, THEN EVALUATED ON CORRESPONDING TESTING DATASETS UNDER NR IQA MODE. BLUE AND GREEN DENOTE NR AND FR DATASETS. OUR PROPOSED YOTO ACHIEVES OUTSTANDING PERFORMANCE ON BOTH FR AND NR JOINT-TRAINING TASKS.

Train	KONIQ + LIVE + CSIQ						LIVEC + TID2013 + KADID					
Test	KONIQ		LIVE		CSIQ		LIVEC		TID2013		KADID	
	PLCC	SROCC	PLCC	SROCC	PLCC	SROCC	PLCC	SROCC	PLCC	SROCC	PLCC	SROCC
Tres	0.764	0.773	0.842	0.839	0.816	0.810	0.702	0.709	0.748	0.731	0.734	0.719
MANIQA	0.828	0.817	0.903	0.898	0.885	0.856	0.871	0.822	0.889	0.882	0.914	0.915
Ours-T	<b>0.866</b>	<b>0.853</b>	<b>0.971</b>	<b>0.972</b>	<b>0.956</b>	<b>0.944</b>	<b>0.912</b>	<b>0.871</b>	<b>0.924</b>	<b>0.923</b>	<b>0.929</b>	<b>0.933</b>

TABLE VIII  
CROSS-DATASET EVALUATION. PART OF THE RESULTS ARE BORROWED FROM [26]. \* STANDS FOR TRANSFORMER-BASED METHODS. THE PROPOSED NETWORK DEMONSTRATES GOOD GENERALIZATION ABILITY.

Mode	FR				Mode	NR			
Train/Test	LIVE / CSIQ		KADID / TID2013		Train/Test	LIVE / CSIQ		KADID / TID2013	
	SROCC	PLCC	SROCC	PLCC		SROCC	PLCC	SROCC	PLCC
WaDIQaM	0.909	0.895	0.834	0.831	TReS	0.652	0.680	0.664	0.639
PieAPP	0.882	0.876	0.859	0.876	MANIQA*	<b>0.788</b>	0.850	0.753	<b>0.763</b>
Ours-FR*	<b>0.917</b>	<b>0.908</b>	<b>0.885</b>	<b>0.889</b>	Ours-NR*	0.782	<b>0.851</b>	<b>0.755</b>	0.762

**Extension to More Modalities** The inclusion of multiple modalities not only enriches the model with additional information but also brings it closer to approximating authentic human experiences in real-life situations. Existing works predominantly engage in the extraction of features from diverse modalities, followed by feature fusion through methods such as hand-crafted rules, pooling, or neural networks to estimate quality scores, as mentioned in [2].

The architecture proposed in this work has the potential to handle multi-modal scenarios. Specifically, for audio-visual IQA, a feasible approach involves feature extraction for each modality for both reference and distorted data, as shown in Fig.9. Features are concatenated channel-wise and then are fed into YOTO. By utilizing self-attention, the importance of

intra-modality features is computed, while cross-attention is employed to ascertain the alignment of inter-modality features. The final step involves leveraging a multi-layer perceptron (MLP) network to estimate quality scores. The actual performance and ablations of the proposed multi-modal architecture await investigation.

**Extension to More Applications** In recent years, the application of IQA has expanded into various domains, including but not limited to Virtual Reality IQA, Light Field IQA, and Screen Content IQA, as mentioned in surveys [43], [71]. Despite the diverse nature of these application scenarios, the fundamental approach to addressing IQA challenges remains remarkably consistent. Broadly speaking, in FR tasks, the core strategy involves a meticulous examination of the disparities

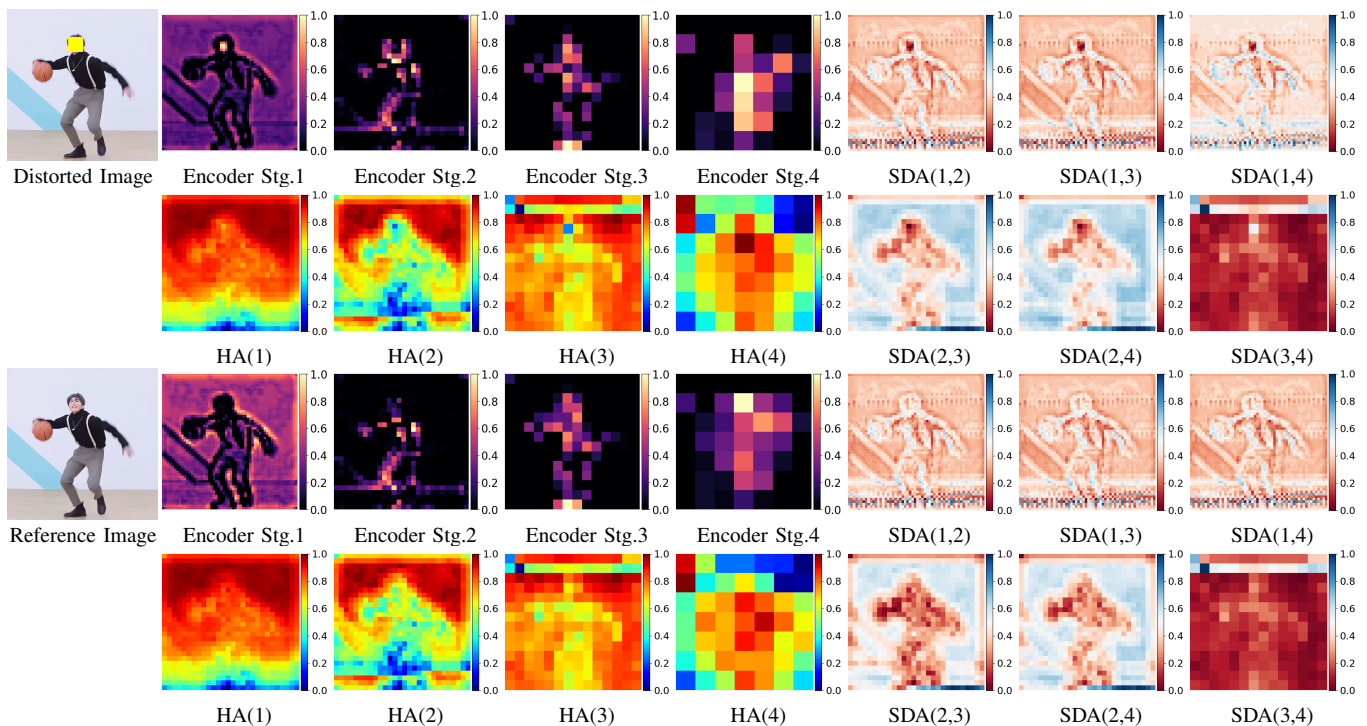


Fig. 7. Illustration of how YOTO detects semantic impact when **Block Occlusion** distortion is presented in a test image in the wild. Features for both distorted and reference images are listed for ease of comparison and a better understanding of each proposed module. ResNet50 is adopted as the encoder backbone. Top half: distorted image and features from encoder stages 1 to 4, HA module, and SDA module are listed respectively. SDA(1,2) denotes cross-attended features between encoder stages 1 and 2. Bottom half: feature maps retrieved at the same position in encoder stages for reference images. It is clear that self-attention is effective in identifying spatial important regions, but lacks consistency across different encoder stages. On the other hand, cross-attention can effectively and consistently reflect similarities between features from different encoder stages, which is beneficial in indicating the residual effect of distortion.

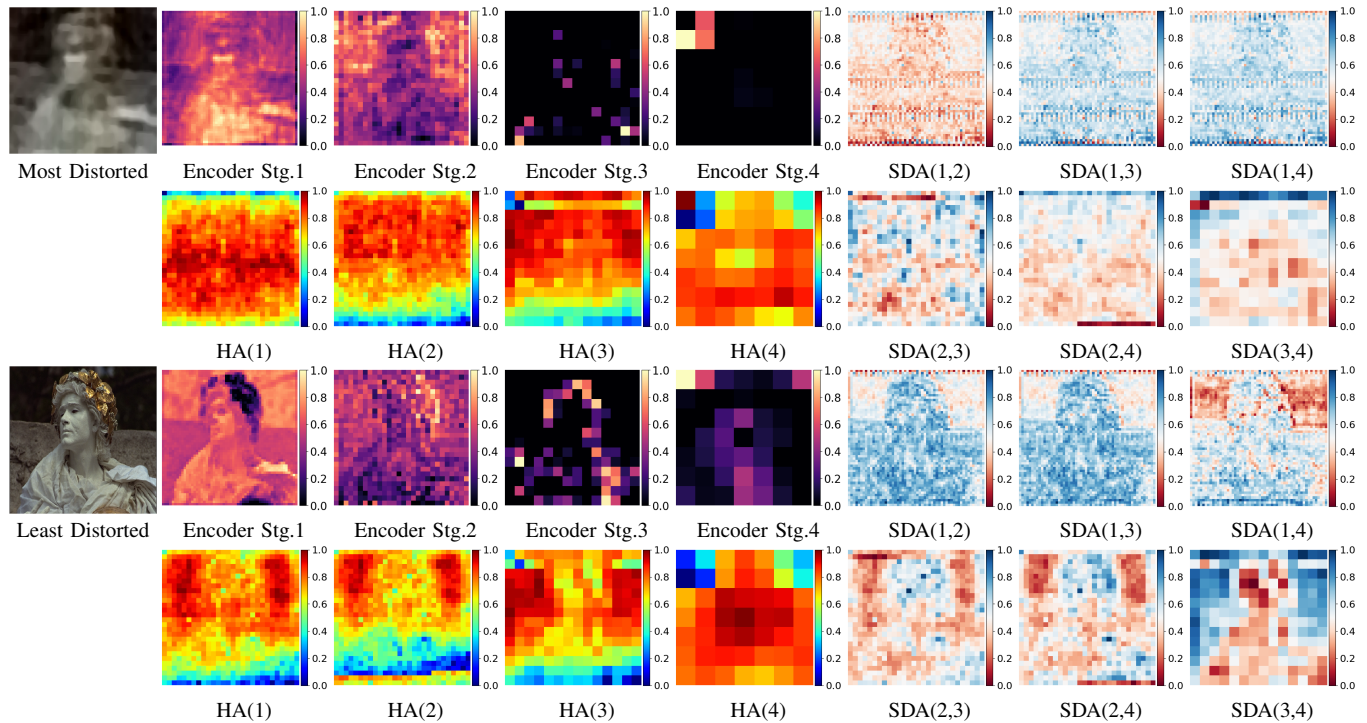


Fig. 8. Illustration of how YOTO detects semantic impact when different levels of **Sparse Sampling** distortion is presented in a test image from TID2013. Similar to Fig. 7, features for the most distorted (level 5) and the least distorted (level 1) images are listed for ease of comparison and a better understanding of each proposed module. ResNet50 is adopted as the encoder backbone. Top half: distortion level 5 and features from encoder stages 1 to 4, HA module, and SDA module are listed respectively. Bottom half: feature maps retrieved at the same position in encoder stages for the least distorted image. As shown above, cross-attention is effective in determining correlations between encoder stages and estimating the semantic impact caused by distortion.

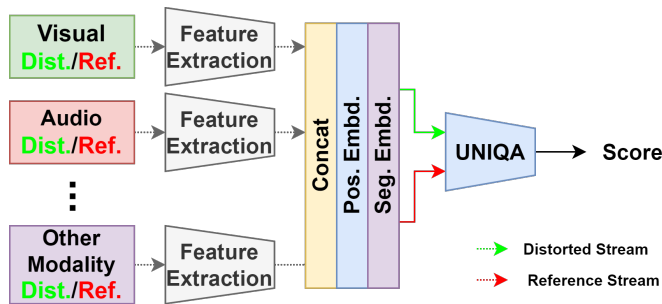


Fig. 9. An illustration of a possible architecture for YOTO when multiple modalities are present for image quality assessment. Feature extraction networks need to be implemented for modality-specific feature extraction. Features from each modality should be treated like RGB images for ease of channel-wise concatenation. After applying position embedding and segment-wise embedding, the proposed YOTO will then perform multi-scale self/cross-attention for quality score prediction.

between a reference image and its distorted counterpart [11], [16], [61]. In NR scenarios, the emphasis shifts towards a nuanced understanding of the inherent data distribution [9], [17], entailing the modeling of data consistency and other pertinent features [10], [20] to holistically evaluate image quality.

The proposed YOTO appears to be promising in terms of its potential for various IQA domains. In the context of traditional IQA and Screen Content IQA, distorted and reference images typically manifest as individual pairs. The proposed YOTO is capable of seamlessly extending to both FR and NR scenarios in such tasks. However, YOTO might not be suitable for Light Field IQA since the prevalent format often involves a collection of images, such as Sub-Aperture Image (SAI), Epipolar Plane Image (EPI), or Micro-lens Array Coded Photograph (MACPI).

## VII. CONCLUSION

In this work, we have proposed a novel architecture based on the transformer and attention mechanism to integrate the FR and NR IQA tasks. To address the input discrepancy between the FR and NR tasks, we introduce a Hierarchical Attention (HA) module that dynamically switches between attention types based on the presence of reference images. Additionally, we partition the attention matrix into blocks at different layers of the HA module to further explore local attention and achieve faster convergence. Considering different types of distortion exhibit varying levels of residual across encoder layers, we devise a Semantic Distortion Aware (SDA) module to capture the similarity between features of different encoder stages. Feature pyramid is split into cones and cross-attention is applied across different layers of each cone. The experimental results demonstrate that our unified framework is capable of handling both FR and NR tasks and achieves overall state-of-the-art results on their respective benchmarks by only being trained once, indicating the effectiveness of the proposed architecture.

## REFERENCES

[1] Da Ai, Yunhong Liu, Yurong Yang, Mingyue Lu, Ying Liu, and Nam Ling. A full-reference image quality assessment method with saliency

and error feature fusion. In *2022 IEEE International Symposium on Circuits and Systems (ISCAS)*, pages 3165–3169, 2022.

[2] Zahid Akhtar and Tiago H. Falk. Audio-visual multimedia quality assessment: A comprehensive survey. *IEEE Access*, 5:21090–21117, 2017.

[3] Sebastian Bosse, Dominique Maniry, Klaus-Robert Müller, Thomas Wiegand, and Wojciech Samek. Deep neural networks for no-reference and full-reference image quality assessment. *IEEE Trans. Image Process.*, 27(1):206–219, 2018.

[4] Sebastian Bosse, Dominique Maniry, Klaus-Robert Müller, Thomas Wiegand, and Wojciech Samek. Deep neural networks for no-reference and full-reference image quality assessment. *IEEE Trans. Image Process.*, 27(1):206–219, 2018.

[5] Baoliang Chen, Lingyu Zhu, Chenqi Kong, Hanwei Zhu, Shiqi Wang, and Zhu Li. No-reference image quality assessment by hallucinating pristine features. *IEEE Transactions on Image Processing*, 31:6139–6151, 2022.

[6] Chun-Fu (Richard) Chen, Quanfu Fan, and Rameswar Panda. Crossvit: Cross-attention multi-scale vision transformer for image classification. In *2021 IEEE/CVF International Conference on Computer Vision, ICCV 2021, Montreal, QC, Canada, October 10-17, 2021*, pages 347–356. IEEE, 2021.

[7] Diqi Chen, Yizhou Wang, and Wen Gao. No-reference image quality assessment: An attention driven approach. *IEEE Transactions on Image Processing*, 29:6496–6506, 2020.

[8] Manri Cheon, Sung-Jun Yoon, Byungyeon Kang, and Junwoo Lee. Perceptual image quality assessment with transformers. In *IEEE Conference on Computer Vision and Pattern Recognition Workshops, CVPR Workshops 2021, virtual, June 19-25, 2021*, pages 433–442. Computer Vision Foundation / IEEE, 2021.

[9] Yuming Fang, Rengang Du, Yifan Zuo, Wenying Wen, and Leida Li. Perceptual quality assessment for screen content images by spatial continuity. *IEEE Trans. Circuits Syst. Video Technol.*, 30(11):4050–4063, 2020.

[10] Yuming Fang, Jiebin Yan, Leida Li, Jinjian Wu, and Weisi Lin. No reference quality assessment for screen content images with both local and global feature representation. *IEEE Trans. Image Process.*, 27(4):1600–1610, 2018.

[11] Ying Fu, Huanqiang Zeng, Lin Ma, Zhangkai Ni, Jianqing Zhu, and Kai-Kuang Ma. Screen content image quality assessment using multi-scale difference of gaussian. *IEEE Trans. Circuits Syst. Video Technol.*, 28(9):2428–2432, 2018.

[12] Deepti Ghadiyaram and Alan C. Bovik. Massive online crowdsourced study of subjective and objective picture quality. *IEEE Trans. Image Process.*, 25(1):372–387, 2016.

[13] Bernd Girod. *What's Wrong with Mean-Squared Error?*, page 207–220. MIT Press, Cambridge, MA, USA, 1993.

[14] S. Alireza Golestaneh, Saba Dadsetan, and Kris M. Kitani. No-reference image quality assessment via transformers, relative ranking, and self-consistency. In *IEEE/CVF Winter Conference on Applications of Computer Vision, WACV 2022, Waikoloa, HI, USA, January 3-8, 2022*, pages 3989–3999. IEEE, 2022.

[15] Jinjin Gu, Haoming Cai, Haoyu Chen, Xiaoxing Ye, Jimmy S. Ren, and Chao Dong. PIPAL: A large-scale image quality assessment dataset for perceptual image restoration. In Andrea Vedaldi, Horst Bischof, Thomas Brox, and Jan-Michael Frahm, editors, *Computer Vision - ECCV 2020 - 16th European Conference, Glasgow, UK, August 23-28, 2020, Proceedings, Part XI*, volume 12356 of *Lecture Notes in Computer Science*, pages 633–651. Springer, 2020.

[16] Ke Gu, Junfei Qiao, Xiongkuo Min, Guanghui Yue, Weisi Lin, and Daniel Thalmann. Evaluating quality of screen content images via structural variation analysis. *IEEE Trans. Vis. Comput. Graph.*, 24(10):2689–2701, 2018.

[17] Ke Gu, Guangtao Zhai, Weisi Lin, Xiaokang Yang, and Wenjun Zhang. Learning a blind quality evaluation engine of screen content images. *Neurocomputing*, 196:140–149, 2016.

[18] Kaiming He, Xiangyu Zhang, Shaoqing Ren, and Jian Sun. Deep residual learning for image recognition. In *2016 IEEE Conference on Computer Vision and Pattern Recognition, CVPR 2016, Las Vegas, NV, USA, June 27-30, 2016*, pages 770–778. IEEE Computer Society, 2016.

[19] Vlad Hosu, Hanhe Lin, Tamás Szirányi, and Dietmar Saupe. Koniq-10k: An ecologically valid database for deep learning of blind image quality assessment. *IEEE Trans. Image Process.*, 29:4041–4056, 2020.

[20] Xuhao Jiang, Liquan Shen, Liangwei Yu, Mingxing Jiang, and Guorui Feng. No-reference screen content image quality assessment based on multi-region features. *Neurocomputing*, 386:30–41, 2020.

[21] Sameulla Khan. Full reference quality assessment of full hd images using combined saliency priors in multi-scale. In *2018 Twenty Fourth National Conference on Communications (NCC)*, pages 1–5, 2018.

- [22] Jongyoo Kim and Sanghoon Lee. Deep learning of human visual sensitivity in image quality assessment framework. In *2017 IEEE Conference on Computer Vision and Pattern Recognition, CVPR 2017, Honolulu, HI, USA, July 21-26, 2017*, pages 1969–1977. IEEE Computer Society, 2017.
- [23] Jongyoo Kim and Sanghoon Lee. Fully deep blind image quality predictor. *IEEE J. Sel. Top. Signal Process.*, 11(1):206–220, 2017.
- [24] Diederik P. Kingma and Jimmy Ba. Adam: A method for stochastic optimization. In Yoshua Bengio and Yann LeCun, editors, *3rd International Conference on Learning Representations, ICLR 2015, San Diego, CA, USA, May 7-9, 2015, Conference Track Proceedings*, 2015.
- [25] Hyunsuk Ko, Dae Yeol Lee, Seunghyun Cho, and Alan C. Bovik. Quality prediction on deep generative images. *IEEE Transactions on Image Processing*, 29:5964–5979, 2020.
- [26] Shanshan Lao, Yuan Gong, Shuwei Shi, Sidi Yang, Tianhe Wu, Jiahao Wang, Weihao Xia, and Yujui Yang. Attentions help cnns see better: Attention-based hybrid image quality assessment network. In *IEEE/CVF Conference on Computer Vision and Pattern Recognition Workshops, CVPR Workshops 2022, New Orleans, LA, USA, June 19-20, 2022*, pages 1139–1148. IEEE, 2022.
- [27] Eric Larson and Damon Chandler. Most apparent distortion: Full-reference image quality assessment and the role of strategy. *J. Electronic Imaging*, 19:011006, 01 2010.
- [28] Kuang-Huei Lee, Xi Chen, Gang Hua, Houdong Hu, and Xiaodong He. Stacked cross attention for image-text matching. In Vittorio Ferrari, Martial Hebert, Cristian Sminchisescu, and Yair Weiss, editors, *Computer Vision - ECCV 2018 - 15th European Conference, Munich, Germany, September 8-14, 2018, Proceedings, Part IV*, volume 11208 of *Lecture Notes in Computer Science*, pages 212–228. Springer, 2018.
- [29] Yang W. Lee, Diane M. Strong, Beverly K. Kahn, and Richard Y. Wang. AIMQ: a methodology for information quality assessment. *Inf. Manag.*, 40(2):133–146, 2002.
- [30] Fan Li, Yangfan Zhang, and Pamela C. Cosman. Mmmnet: An end-to-end multi-task deep convolution neural network with multi-scale and multi-hierarchy fusion for blind image quality assessment. *IEEE Transactions on Circuits and Systems for Video Technology*, 31(12):4798–4811, 2021.
- [31] Hezheng Lin, Xing Cheng, Xiangyu Wu, and Dong Shen. CAT: cross attention in vision transformer. In *IEEE International Conference on Multimedia and Expo, ICME 2022, Taipei, Taiwan, July 18-22, 2022*, pages 1–6. IEEE, 2022.
- [32] Hanhe Lin, Vlad Hosu, and Dietmar Saupe. Kadid-10k: A large-scale artificially distorted IQA database. In *11th International Conference on Quality of Multimedia Experience QoMEX 2019, Berlin, Germany, June 5-7, 2019*, pages 1–3. IEEE, 2019.
- [33] Kwan-Yee Lin and Guanxiang Wang. Hallucinated-iqa: No-reference image quality assessment via adversarial learning. In *2018 IEEE Conference on Computer Vision and Pattern Recognition, CVPR 2018, Salt Lake City, UT, USA, June 18-22, 2018*, pages 732–741. Computer Vision Foundation / IEEE Computer Society, 2018.
- [34] Weisi Lin and C.-C. Jay Kuo. Perceptual visual quality metrics: A survey. *Journal of Visual Communication and Image Representation*, 22(4):297–312, 2011.
- [35] Manni Liu, Jiabin Huang, Delu Zeng, Xinghao Ding, and John Paisley. A multiscale approach to deep blind image quality assessment. *IEEE Transactions on Image Processing*, 32:1656–1667, 2023.
- [36] Xialei Liu, Joost van de Weijer, and Andrew D. Bagdanov. Rankiqa: Learning from rankings for no-reference image quality assessment. In *IEEE International Conference on Computer Vision, ICCV 2017, Venice, Italy, October 22-29, 2017*, pages 1040–1049. IEEE Computer Society, 2017.
- [37] Ze Liu, Yutong Lin, Yue Cao, Han Hu, Yixuan Wei, Zheng Zhang, Stephen Lin, and Baining Guo. Swin transformer: Hierarchical vision transformer using shifted windows. In *2021 IEEE/CVF International Conference on Computer Vision, ICCV 2021, Montreal, QC, Canada, October 10-17, 2021*, pages 9992–10002. IEEE, 2021.
- [38] Yihang Lou, Yan Bai, Jun Liu, Shiqi Wang, and Lingyu Duan. Veri-wild: A large dataset and a new method for vehicle re-identification in the wild. In *IEEE Conference on Computer Vision and Pattern Recognition, CVPR 2019, Long Beach, CA, USA, June 16-20, 2019*, pages 3235–3243. Computer Vision Foundation / IEEE, 2019.
- [39] Jupu Ma, Jinjian Wu, Leida Li, Weisheng Dong, Xuemei Xie, Guangming Shi, and Weisi Lin. Blind image quality assessment with active inference. *IEEE Trans. Image Process.*, 30:3650–3663, 2021.
- [40] Kede Ma, Wentao Liu, Kai Zhang, Zhengfang Duanmu, Zhou Wang, and Wangmeng Zuo. End-to-end blind image quality assessment using deep neural networks. *IEEE Trans. Image Process.*, 27(3):1202–1213, 2018.
- [41] Pavan C. Madhusudana, Neil Birkbeck, Yilin Wang, Balu Adsumilli, and Alan C. Bovik. Image quality assessment using contrastive learning. *IEEE Transactions on Image Processing*, 31:4149–4161, 2022.
- [42] Xiongkuo Min, Ke Gu, Guangtao Zhai, Jing Liu, Xiaokang Yang, and Chang Wen Chen. Blind quality assessment based on pseudo-reference image. *IEEE Transactions on Multimedia*, 20(8):2049–2062, 2018.
- [43] Xiongkuo Min, Ke Gu, Guangtao Zhai, Xiaokang Yang, Wenjun Zhang, Patrick Le Callet, and Chang Wen Chen. Screen content quality assessment: Overview, benchmark, and beyond. *ACM Comput. Surv.*, 54(9), oct 2021.
- [44] Xiongkuo Min, Guangtao Zhai, Ke Gu, Yutao Liu, and Xiaokang Yang. Blind image quality estimation via distortion aggravation. *IEEE Transactions on Broadcasting*, 64(2):508–517, 2018.
- [45] Xiongkuo Min, Guangtao Zhai, Jiantao Zhou, Mylène C. Q. Farias, and Alan Conrad Bovik. Study of subjective and objective quality assessment of audio-visual signals. *IEEE Trans. Image Process.*, 29:6054–6068, 2020.
- [46] Xiongkuo Min, Guangtao Zhai, Jiantao Zhou, Xiao-Ping (Steven) Zhang, Xiaokang Yang, and Xiping Guan. A multimodal saliency model for videos with high audio-visual correspondence. *IEEE Trans. Image Process.*, 29:3805–3819, 2020.
- [47] Anish Mittal, Anush Krishna Moorthy, and Alan Conrad Bovik. No-reference image quality assessment in the spatial domain. *IEEE Trans. Image Process.*, 21(12):4695–4708, 2012.
- [48] Fu-Zhao Ou, Yuan-Gen Wang, Jin Li, Guopu Zhu, and Sam Kwong. A novel rank learning based no-reference image quality assessment method. *IEEE Transactions on Multimedia*, 24:4197–4211, 2022.
- [49] Zhaoqing Pan, Hao Zhang, Jianjun Lei, Yuming Fang, Xiao Shao, Nam Ling, and Sam Kwong. Dacnn: Blind image quality assessment via a distortion-aware convolutional neural network. *IEEE Transactions on Circuits and Systems for Video Technology*, 32(11):7518–7531, 2022.
- [50] Soo-Chang Pei and Li-Heng Chen. Image quality assessment using human visual DOG model fused with random forest. *IEEE Trans. Image Process.*, 24(11):3282–3292, 2015.
- [51] Nikolay N. Ponomarenko, Lina Jin, Oleg Jeremeiev, Vladimir V. Lukin, Karen O. Egiazarian, Jaakko Astola, Benoît Vozel, Kacem Chehdi, Marco Carli, Federica Battisti, and C.-C. Jay Kuo. Image database TID2013: peculiarities, results and perspectives. *Signal Process. Image Commun.*, 30:57–77, 2015.
- [52] Ekta Prashnani, Hong Cai, Yasamin Mostofi, and Pradeep Sen. Pieapp: Perceptual image-error assessment through pairwise preference. In *2018 IEEE Conference on Computer Vision and Pattern Recognition, CVPR 2018, Salt Lake City, UT, USA, June 18-22, 2018*, pages 1808–1817. Computer Vision Foundation / IEEE Computer Society, 2018.
- [53] Michele A. Saad, Alan C. Bovik, and Christophe Charrier. Blind image quality assessment: A natural scene statistics approach in the DCT domain. *IEEE Trans. Image Process.*, 21(8):3339–3352, 2012.
- [54] Soomin Seo, Sehwan Ki, and Munchurl Kim. A novel just-noticeable-difference-based saliency-channel attention residual network for full-reference image quality predictions. *IEEE Trans. Circuits Syst. Video Technol.*, 31(7):2602–2616, 2021.
- [55] H. R. Sheikh, Z. Wang, L. Cormack, and A. C. Bovik. Live image quality assessment database release 2. , 2015.
- [56] Shaolin Su, Qingsen Yan, Yu Zhu, Cheng Zhang, Xin Ge, Jinqiu Sun, and Yanning Zhang. Blindly assess image quality in the wild guided by a self-adaptive hyper network. In *2020 IEEE/CVF Conference on Computer Vision and Pattern Recognition, CVPR 2020, Seattle, WA, USA, June 13-19, 2020*, pages 3664–3673. Computer Vision Foundation / IEEE, 2020.
- [57] Wei Sun, Huiyu Duan, Xiongkuo Min, Li Chen, and Guangtao Zhai. Blind quality assessment for in-the-wild images via hierarchical feature fusion strategy. In *2022 IEEE International Symposium on Broadband Multimedia Systems and Broadcasting (BMSB)*, pages 01–06, 2022.
- [58] Domonkos Varga. Composition-preserving deep approach to full-reference image quality assessment. *Signal Image Video Process.*, 14(6):1265–1272, 2020.
- [59] Ashish Vaswani, Noam Shazeer, Niki Parmar, Jakob Uszkoreit, Llion Jones, Aidan N. Gomez, Lukasz Kaiser, and Illia Polosukhin. Attention is all you need. In Isabelle Guyon, Ulrike von Luxburg, Samy Bengio, Hanna M. Wallach, Rob Fergus, S. V. N. Vishwanathan, and Roman Garnett, editors, *Advances in Neural Information Processing Systems 30: Annual Conference on Neural Information Processing Systems 2017, December 4-9, 2017, Long Beach, CA, USA*, pages 5998–6008, 2017.
- [60] Jing Wang, Haotian Fan, Xiaoxia Hou, Yitian Xu, Tao Li, Xuechao Lu, and Lean Fu. MSTRIQ: no reference image quality assessment based on swin transformer with multi-stage fusion. In *IEEE/CVF Conference on Computer Vision and Pattern Recognition Workshops, CVPR Workshops 2022, New Orleans, LA, USA, June 19-20, 2022*, pages 1268–1277. IEEE, 2022.
- [61] Ruifeng Wang, Huan Yang, Zhenkuan Pan, Baoxiang Huang, and Guojia



- Hou. Screen content image quality assessment with edge features in gradient domain. *IEEE Access*, 7:5285–5295, 2019.
- [62] Zhou Wang, Alan C. Bovik, Hamid R. Sheikh, and Eero P. Simoncelli. Image quality assessment: from error visibility to structural similarity. *IEEE Trans. Image Process.*, 13(4):600–612, 2004.
- [63] Zhihua Wang, Qiuping Jiang, Shanshan Zhao, Wensen Feng, and Weisi Lin. Deep blind image quality assessment powered by online hard example mining. *IEEE Transactions on Multimedia*, pages 1–11, 2023.
- [64] Xi Wei, Tianzhu Zhang, Yan Li, Yongdong Zhang, and Feng Wu. Multimodality cross attention network for image and sentence matching. In *2020 IEEE/CVF Conference on Computer Vision and Pattern Recognition, CVPR 2020, Seattle, WA, USA, June 13-19, 2020*, pages 10938–10947. Computer Vision Foundation / IEEE, 2020.
- [65] Jinjian Wu, Jupao Ma, Fuhu Liang, Weisheng Dong, Guangming Shi, and Weisi Lin. End-to-end blind image quality prediction with cascaded deep neural network. *IEEE Transactions on Image Processing*, 29:7414–7426, 2020.
- [66] Sheng Yang, Qiuping Jiang, Weisi Lin, and Yongtao Wang. Sgdnet: An end-to-end saliency-guided deep neural network for no-reference image quality assessment. In *Proceedings of the 27th ACM International Conference on Multimedia, MM '19*, page 1383–1391, New York, NY, USA, 2019. Association for Computing Machinery.
- [67] Sidi Yang, Tianhe Wu, Shuwei Shi, Shanshan Lao, Yuan Gong, Mingdeng Cao, Jiahao Wang, and Yujiu Yang. MANIQA: multi-dimension attention network for no-reference image quality assessment. In *IEEE/CVF Conference on Computer Vision and Pattern Recognition Workshops, CVPR Workshops 2022, New Orleans, LA, USA, June 19-20, 2022*, pages 1190–1199. IEEE, 2022.
- [68] Zhenqiang Ying, Haoran Niu, Praful Gupta, Dhruv Mahajan, Deepti Ghadiyaram, and Alan C. Bovik. From patches to pictures (paq-2-piq): Mapping the perceptual space of picture quality. In *2020 IEEE/CVF Conference on Computer Vision and Pattern Recognition, CVPR 2020, Seattle, WA, USA, June 13-19, 2020*, pages 3572–3582. Computer Vision Foundation / IEEE, 2020.
- [69] Zhenqiang Ying, Haoran Niu, Praful Gupta, Dhruv Mahajan, Deepti Ghadiyaram, and Alan C. Bovik. From patches to pictures (paq-2-piq): Mapping the perceptual space of picture quality. In *2020 IEEE/CVF Conference on Computer Vision and Pattern Recognition, CVPR 2020, Seattle, WA, USA, June 13-19, 2020*, pages 3572–3582. Computer Vision Foundation / IEEE, 2020.
- [70] Junyong You and Jari Korhonen. Transformer for image quality assessment. In *2021 IEEE International Conference on Image Processing, ICIP 2021, Anchorage, AK, USA, September 19-22, 2021*, pages 1389–1393. IEEE, 2021.
- [71] Guangtao Zhai and Xiongkuo Min. Perceptual image quality assessment: a survey. *Sci. China Inf. Sci.*, 63(11), 2020.
- [72] Lin Zhang, Lei Zhang, and Alan C. Bovik. A feature-enriched completely blind image quality evaluator. *IEEE Trans. Image Process.*, 24(8):2579–2591, 2015.
- [73] Min Zhang, Xuanqin Mou, and Lei Zhang. Non-shift edge based ratio (NSER): an image quality assessment metric based on early vision features. *IEEE Signal Process. Lett.*, 18(5):315–318, 2011.
- [74] Weixia Zhang, Kede Ma, Jia Yan, Dexiang Deng, and Zhou Wang. Blind image quality assessment using a deep bilinear convolutional neural network. *IEEE Trans. Circuits Syst. Video Technol.*, 30(1):36–47, 2020.
- [75] Qiangqiang Zhou, Xianhui Liu, Lin Zhang, Weidong Zhao, and Yufei Chen. Saliency-based image quality assessment metric. In *2016 3rd International Conference on Systems and Informatics (ICSAI)*, pages 918–924, 2016.
- [76] Hancheng Zhu, Leida Li, Jinjian Wu, Weisheng Dong, and Guangming Shi. Metaiqa: Deep meta-learning for no-reference image quality assessment. In *2020 IEEE/CVF Conference on Computer Vision and Pattern Recognition, CVPR 2020, Seattle, WA, USA, June 13-19, 2020*, pages 14131–14140. Computer Vision Foundation / IEEE, 2020.
- [77] Yucheng Zhu, Yunhao Li, Wei Sun, Xiongkuo Min, Guangtao Zhai, and Xiaokang Yang. Blind image quality assessment via cross-view consistency. *IEEE Transactions on Multimedia*, pages 1–14, 2022.
- [78] Zhe Zhu, Dun Liang, Song-Hai Zhang, Xiaolei Huang, Baoli Li, and Shi-Min Hu. Traffic-sign detection and classification in the wild. In *2016 IEEE Conference on Computer Vision and Pattern Recognition, CVPR 2016, Las Vegas, NV, USA, June 27-30, 2016*, pages 2110–2118. IEEE Computer Society, 2016.